A Parametric Magneto-Dynamic Model of Soft Magnetic Steel Sheets

Martin Petrun[1], Vojko Podlogar[1], Simon Steentjes[2], Kay Hameyer[2], and Drago Dolinar[1]

[1]Institute of Power Engineering, FERI, University of Maribor, Maribor SI-2000, Slovenia
[2]Institute of Electrical Machines, RWTH Aachen University, Aachen D-52062, Germany

This paper deals with a new analytical parametric magneto-dynamic model of a thin soft magnetic steel sheet (SMSS). The interdependence of the magnetic field and eddy currents inside such an SMSS is calculated by dividing the sheets into an arbitrary number of slices. Using an adequate number of slices, the magnetic field and eddy currents are described piece-wise uniformly across the SMSS for a given excitation dynamics. Dynamic hysteresis loops for arbitrary excitations can be calculated using the proposed model. The calculated results are validated by the measurements on a non-oriented SMSS.

Index Terms—**Dynamic modeling, eddy currents, magnetic hysteresis, soft magnetic materials.**

I. Introduction

SOFT magnetic steel sheets (SMSSs) represent an important integral part of many electromagnetic devices and seem to be almost irreplaceable in the process of electromagnetic energy conversion. The widespread usages of SMSSs have created the need for adequate descriptions of the magnetization processes and loss mechanisms in an SMSS, but despite this problem having already been investigated for decades, it can still be considered as unsolved and is representing one of the biggest challenges in electrical engineering and physics. Inside a thin non-oriented (NO) SMSS with predominately small magnetic domains, eddy currents are modeled parallel to the surface of the SMSS [1]. This problem is usually solved by using the well-known 1-D Maxwell penetration equation, which links the magnetic field strength H and the magnetic flux density B in a homogenous SMSS [1], [2]. Solving the penetration equation is however complicated, limited to certain hysteresis models, and requires numerically intensive solving methods (e.g., finite differences).

The aim of this paper is to develop a dynamic model which describes the interdependencies between magnetic field and eddy currents inside a thin SMSS. The proposed magneto-dynamic model is based on the methodology used for the iron core model presented in [3]. Such methodology is promising from the engineering standpoint as it is relatively simple, provides very good results for the application presented in [3], and is with further development easy to implement. The magneto-dynamic model is coupled with an external electric excitation circuit and enables the predicting of dynamic hysteresis curves under arbitrary magnetization conditions. The presented model is evaluated on a NO SMSS, where very good results within a wide frequency range are obtained.

II. Magneto-Dynamic Model of an SMSS

The presented magneto-dynamic model is based on Ampere and Faraday Laws. Fig. 1 shows a thin and long SMSS, where

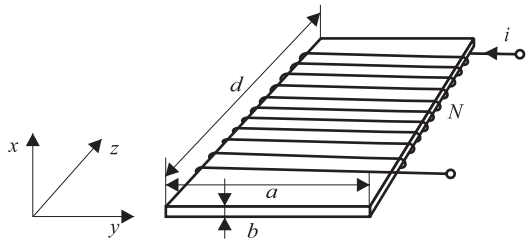

Fig. 1. Long straight SMSS.

a is the width, b is the thickness, d is the length of the SMSS, N is the number of turns of the winding, and i is the excitation current.

The magnetic field inside the SMSS shown in Fig. 1 is excited with a magneto-motive force (mmf) Θ caused by the current i in a winding with N turns

$$\Theta(t) = N \cdot i(t). \tag{1}$$

Assuming that $d \gg a \gg b$, the discussed SMSS can be treated as infinitely long, where the magnetic field on the edges has a negligible effect on the magnetic field inside the SMSS. The magnetic field in the SMSS can therefore simply be represented just by its longitudinal component (in the direction of z-axis), while other components can be neglected.

The magnetic field inside such an SMSS can be treated as uniform when the dynamic of the excitation current i is adequately low. This assumption holds true when the SMSS thickness b is smaller than the penetration depth δ of the magnetic field produced by the excitation winding. In such cases, the influence of eddy currents on the magnetic field is considered by the classical eddy-current factor $\sigma b^2/12$ [3], [4], where σ is the specific electrical conductivity of the SMSS.

A. Influence of Eddy-Currents on Magnetic Field Distribution Inside an SMSS

Using higher excitation dynamics, the influence of eddy currents on magnetic field distribution inside an SMSS becomes significant and the magnetic field cannot be treated as uniform anymore. However, the magnetic field distribution can be described piece-wise uniformly across the SMSS thickness by dividing the SMSS into several slices. Such a methodology is used for the modeling of an iron core [3]. When dividing

Manuscript received August 7, 2013; revised October 10, 2013; accepted October 20, 2013. Date of current version April 4, 2014. Corresponding author: M. Petrun (e-mail: martin.petrun@um.si).

Color versions of one or more of the figures in this paper are available online at http://ieeexplore.ieee.org.

Digital Object Identifier 10.1109/TMAG.2013.2288304

the SMSS into an adequate number of slices N_s, the magnetic field inside the individual slices can be treated as uniform. It is assumed that the first slice ($s = 1$) is in the middle and last slice ($s = N_s$) on the edge of the SMSS [3].

Let s be an arbitrary slice in the discussed SMSS. Assuming that the magnetic field in the observed slice s is almost uniform, it can be described by its average value of magnetic field strength $\bar{H}_s$ (2) and magnetic flux density $\bar{B}_s$ (3), since the deviations between the calculated average values and real values are negligible

$$\bar{H}_s = \frac{2N_s}{b} \int_{\frac{(s-1)b}{2N_s}}^{\frac{sb}{2N_s}} H_s(x)\, dx, \qquad s \in N_s \tag{2}$$

$$\bar{B}_s = \frac{2N_s}{b} \int_{\frac{(s-1)b}{2N_s}}^{\frac{sb}{2N_s}} B_s(x)\, dx, \qquad s \in N_s. \tag{3}$$

The eddy current density $j_{eys}(x)$ along the y-axis in the slice s is calculated by (4). The first term on the right side of (4) represents the contributions of the varying magnetic fields within the embraced inner slices, whereas the second term on the right side describes the contribution of the varying magnetic field in slice s

$$j_{eys}(x) = -\sigma \frac{b}{2N_s} \sum_{i=1}^{s-1} \frac{d\bar{B}_i}{dt} - \sigma \frac{d\bar{B}_s}{dt} \left(x - \frac{(s-1)b}{2N_s} \right). \tag{4}$$

Integrating (4) across the observed slice s, the eddy current i_{es} in slice s is calculated by (5), where l_m represents the mean length of the SMSS. This eddy current i_{es} is induced by the change of average magnetic flux densities in inner slices $\bar{B}_i$ and partially by the change of magnetic flux $\bar{B}_s$ in the observed slice s

$$i_{es} = -c \left(\sum_{i=1}^{s-1} \frac{d\bar{B}_i}{dt} + \frac{1}{2} \frac{d\bar{B}_s}{dt} \right), c = \sigma l_m \left(\frac{b}{2N_s} \right)^2. \tag{5}$$

Using Ampere's Law, the mmf balance for slice s is expressed as (6). The magnetic field inside slice s is excited by the externally applied mmf Θ, the eddy currents that enclose the slice s [second term on the right side of (6)], and also that part of the eddy current enclosing the observed magnetic field [last two terms on the right side of (6)]

$$H_s(x)\, l_m = \Theta + \sum_{i=s+1}^{N_s} i_{ei} + \left(i_{es} - i_{eys}(x) \right). \tag{6}$$

Following integration of (6) over the thickness of the slice s, the mmf balance in the slice s is expressed by (7) with average magnetic field strength (2) and average flux density (3) in the slice s, and the sum of the eddy currents (5) in all the slices

$$\bar{H}_s\left(\bar{B}_s\right) l_m = \Theta + \sum_{i=s+1}^{N_s} i_{ei} + \frac{2}{3} i_{es} + \frac{1}{3} \sum_{i=1}^{s-1} (-1)^{s+i}\, i_{ei}. \tag{7}$$

When considering all the slices, the mmf balance for the whole SMSS is expressed in matrix form by

$$\bar{\mathbf{H}}(\bar{\mathbf{B}}) l_m = \boldsymbol{\Theta} + \boldsymbol{\Theta}_e \tag{8}$$

where $\bar{\mathbf{H}}(\bar{\mathbf{B}})$ is a vector of the magnetic field strengths as nonlinear (hysteresis) functions of the magnetic flux densities inside individual slices, and $\boldsymbol{\Theta}$ is the vector of mmfs caused by the externally applied current i. This vector contains equal values ($\boldsymbol{\Theta} = \mathbf{N}i; \mathbf{N} = N[1]_{N_s \times 1}$), as all of the slices of the SMSS are enclosed and excited with the same externally applied mmf (1). The vector $\boldsymbol{\Theta}_e$ of mmf in (8) is caused by eddy currents and is, according to (7), given in matrix form by

$$\boldsymbol{\Theta}_e = \frac{1}{3} \begin{bmatrix} 2 & 3 & 3 & \cdots & 3 & 3 \\ -1 & 2 & 3 & \cdots & 3 & 3 \\ +1 & -1 & 2 & \cdots & 3 & 3 \\ \vdots & \vdots & \vdots & \ddots & \vdots & \vdots \\ \mp 1 & \pm 1 & \mp 1 & \cdots & 2 & 3 \\ \pm 1 & \mp 1 & \pm 1 & \cdots & \mp 1 & 2 \end{bmatrix} \begin{bmatrix} i_{e1} \\ i_{e2} \\ \vdots \\ i_{eNs} \end{bmatrix} = \mathbf{A}_1 \mathbf{i}_e. \tag{9}$$

The vector of eddy currents of individual slices $\mathbf{i}_e$ in (9) is calculated according to (5) by (10), where $\bar{\mathbf{B}}$ is a vector of the average magnetic flux densities in the slices and $\mathbf{A}_2$ is a linear matrix representing the contributions of the varying magnetic fields to the eddy currents

$$\begin{bmatrix} i_{e1} \\ i_{e2} \\ \vdots \\ i_{eNs} \end{bmatrix} = -\frac{c}{2} \begin{bmatrix} 1 & 0 & \cdots & 0 & 0 \\ 2 & 1 & \cdots & 0 & 0 \\ \vdots & \vdots & \ddots & \vdots & \vdots \\ 2 & 2 & \cdots & 1 & 0 \\ 2 & 2 & \cdots & 2 & 1 \end{bmatrix} \frac{d}{dt} \begin{bmatrix} \bar{B}_1 \\ \bar{B}_2 \\ \vdots \\ \bar{B}_{Ns} \end{bmatrix} = -\mathbf{A}_2 \frac{d}{dt} \bar{\mathbf{B}}. \tag{10}$$

Using (8)–(10), joining (9) and (10), and by considering $\boldsymbol{\Phi} = (A_{Fe}/N_s)\bar{\mathbf{B}}$, where A_{Fe} is the effective cross section of the SMSS, the mmf balance in the SMSS is expressed as

$$\bar{\mathbf{H}}\left(\bar{\boldsymbol{\Phi}}\right) l_m = \boldsymbol{\Theta} + \mathbf{A}_1 (-\mathbf{A}_2) \frac{N_s}{A_{Fe}} \frac{d}{dt} \boldsymbol{\Phi}. \tag{11}$$

Rearranging (11) and by considering $\mathbf{L}_m = \mathbf{A}_1 \mathbf{A}_2 N_s / A_{Fe}$ (12) is obtained, where by analogy to electric circuits $\mathbf{L}_m$ represents the so-called linear magnetic tensor inductance matrix of the SMSS. The total mmf $\boldsymbol{\Theta}$ in the SMSS is, according to (12), a sum of mmfs $\boldsymbol{\Theta}_{Rm}$ (caused by static hysteresis of individual slices) and $\boldsymbol{\Theta}_{Lm}$ (caused by eddy currents inside the SMSS)

$$\boldsymbol{\Theta} = \mathbf{N}i = \bar{\mathbf{H}}\left(\bar{\boldsymbol{\Phi}}\right) l_m + \mathbf{L}_m \frac{d\boldsymbol{\Phi}}{dt} = \boldsymbol{\Theta}_{Rm} + \boldsymbol{\Theta}_{Lm}. \tag{12}$$

Based on Faraday's Law, the average magnetic flux Φ_m in the SMSS couples magnetic (12) and electrical (13) subsystems. This coupling completes the interdependence between magnetic field and eddy current distributions inside the SMSS, and induced voltage u_i in the excitation winding

$$u_i = -N \frac{d\Phi_m(\boldsymbol{\Theta})}{dt} = -\mathbf{N}^T \frac{d}{dt} \left(\frac{A_{Fe}}{N_s} \bar{\mathbf{B}} \right). \tag{13}$$

B. Nonlinear Properties of SMSSs

To completely describe the discussed magneto-dynamic model of an SMSS, the nonlinear relationship between H_s and B_s in each individual slice s has to be taken into account. For this purpose various hysteresis models can be implemented,

TABLE I
M400-50A NO SMSS AND MODEL DATA

Parameter	Quantity	Value
A_{Fe}	effective cross section	15 mm^2
l_m	mean magnetic path length	940 mm
b	thickness	0.5 mm
a	width	30 mm
σ	specific electrical conductivity	$2.16 \cdot 10^6$ S/m

see [2], [4]–[8]. The chosen hysteresis model describes the static hysteresis relationship $H_s(B_s)$ of each individual slice s, which can be determined from quasi static measurements or datasheets of the modeled SMSS. The choice of the implemented hysteresis model also affects the accuracy and performance of the presented magneto-dynamic model, since its performance depends on the accuracy and complexity of the used static hysteresis model. In this paper the hysteresis model proposed by Tellinen [4] was implemented for several practical reasons. This hysteresis model is, despite being relatively simple, reasonably accurate, computationally inexpensive, and also easy to implement. The main advantage and motivation for using this model in this paper was that the model is based on the measured major static hysteresis loop of the SMSS in the form of a look-up table. Consequently the used model adequately describes major static hysteresis loops with irregular shapes. Such irregular shapes are typical for the static hysteresis loops of NO steels [2]. Although there are several other developed hysteresis models [4]–[8], some of them have troubles recreating static hysteresis loops with irregular shapes or have challenging parameter identification and implementation. Furthermore, for the analysis of complex magnetizations a history-dependent hysteresis model could be used, e.g., the hysteresis model proposed in [2].

The static hysteresis model along with (12) and (13) completely describe the parametric magneto-dynamic model of an SMSS, which can be coupled with an external excitation circuit lumped parameter model. Using presented model the eddy current and hysteresis losses can also be calculated, which is presented in [3].

III. RESULTS

The discussed magneto-dynamic model was validated by comparing the calculated and measured major and symmetrical minor dynamic hysteresis loops for a M400-50A NO steel. The experimental results for the presented evaluation were carried out on an Epstein frame, which was incorporated into an accurate computer controlled system. The SMSS sample was characterized using controlled sinusoidal magnetic flux density with a form factor error of less than 1% in the frequency range from quasi-static to 1000 Hz. In Table I the data of the measured SMSS and of the discussed parametric magneto-dynamic model are shown.

The comparison between the measured and calculated dynamic hysteresis for different peak average magnetic flux densities B_{max} (0.6, 0.9, 1.2, and 1.5 T) at two different frequencies f (400 and 1000 Hz) along with the static hysteresis loop in the SMSS, is shown in Fig. 2.

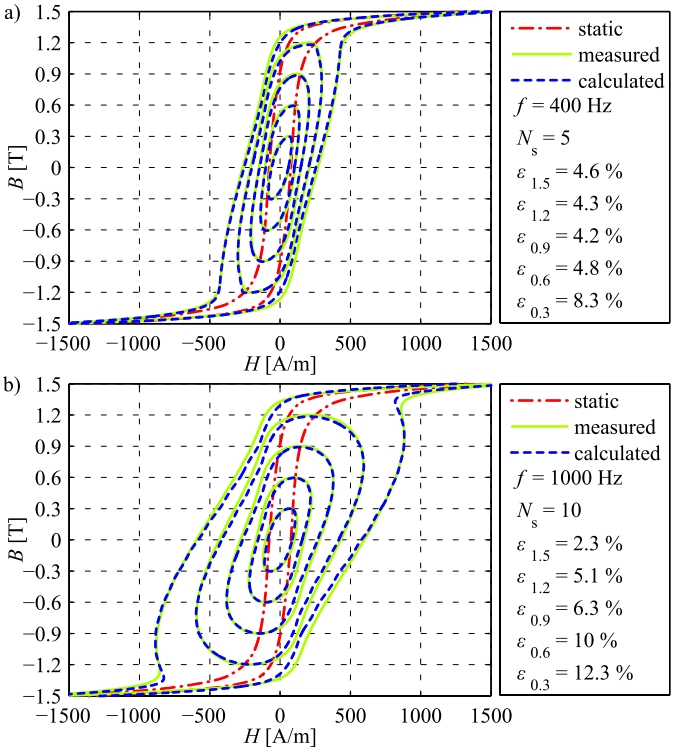

Fig. 2. Measured static and dynamic hysteresis loops compared to calculated dynamic hysteresis loops at different maximum average magnetic flux densities B_{max} for excitation frequencies: a) $f = 400$ Hz and b) $f = 1000$ Hz.

The calculated results show a very good shape agreement with the measurements within the whole tested frequency range using constant model parameters, only the number of slices N_s was adapted according to excitation frequency in order to achieve good accuracy and computational performance. The computation time for one period using a non-optimized code in MATLAB R2009b on a desktop computer ranged from a couple of seconds at low maximum average flux densities B_{max} and low number of slices N_s to approximately a minute at $B_{max} = 1.5$ T, $f = 1000$ Hz, and $N_s = 10$. The calculated relative deviations of the loop areas ε increased slightly at low B_{max} due to the slightly lower accuracy of the used static hysteresis model at low B_{max}.

The calculated magnetic flux densities $B(t)$ and corresponding eddy currents $i_{es}(t)$ at $f = 1000$ Hz are for one time period shown in Figs. 3 and 4, respectively. Fig. 3(a) and Fig. 4(a) correspond to the maximum average flux density $B_{max} = 0.6$ T, whereas Fig. 3(b) and Fig. 4(b) correspond to $B_{max} = 1.5$ T inside the M400-50A SMSS. Only the results for slices 1, 4, 7, and 10 are shown because of better transparency. The calculated results show a strong influence of the eddy currents i_{es} on the magnetic field B_{si} inside the SMSS. At average flux density of $B_{max} = 0.6$ T the skin effect of the magnetic field inside the observed SMSS is severe, as the peak magnetic flux density B_{maxs} in individual slices varies by a factor of 6. Also a phase shift is observed between the magnetic flux densities B_{si} inside the different slices.

However, when the average magnetic flux density inside SMSS approaches saturation, the skin effect

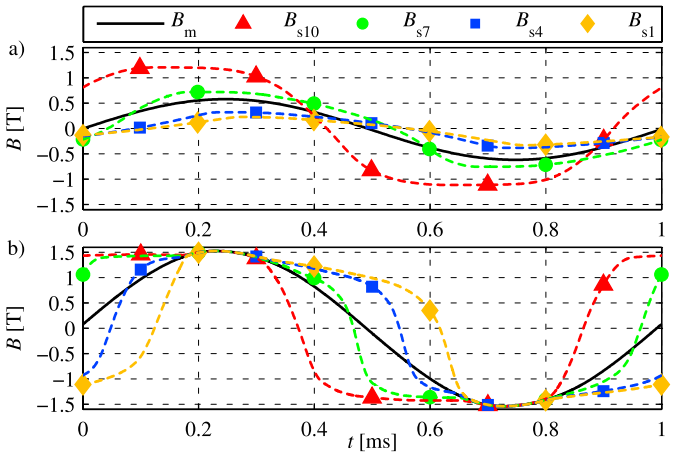

Fig. 3. Calculated magnetic flux densities B_s in slices $s = 1$, 4, 7, and 10, along with the average magnetic flux density B_m inside the M400-50A NO SMSS for $N_s = 10$ and $f = 1000$ Hz: (a) $B_{max} = 0.6$ T and (b) $B_{max} = 1.5$ T.

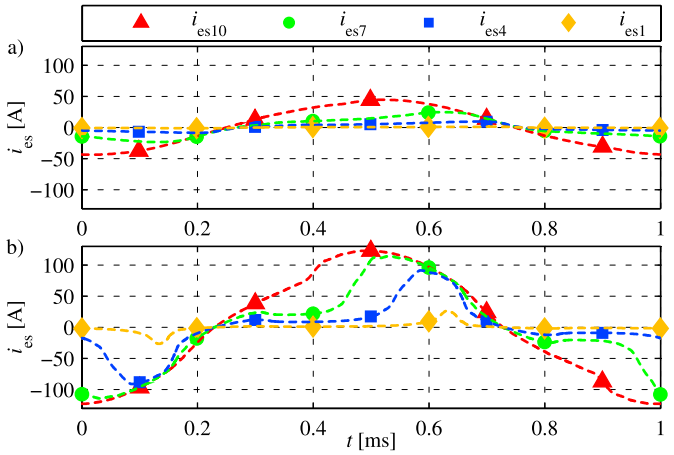

Fig. 4. Calculated eddy currents i_{es} in slices $s = 1, 4, 7$, and 10 inside the M400-50A NO SMSS for $N_s = 10$ and $f = 1000$ Hz: (a) $B_{max} = 0.6$ T and (b) $B_{max} = 1.5$ T.

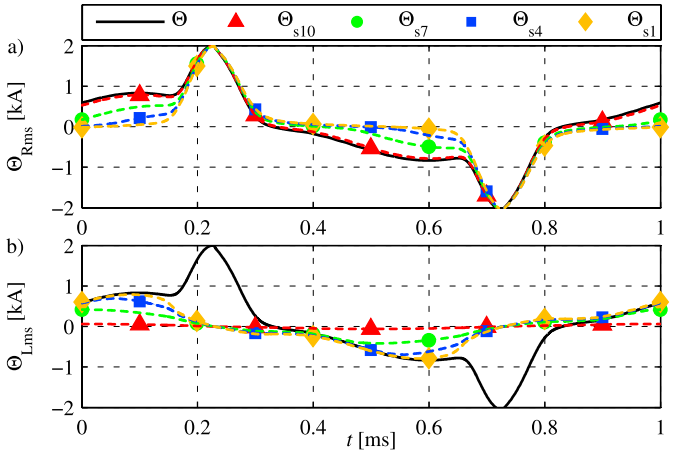

Fig. 5. Calculated mmfs in slices $s = 1, 4, 7$, and 10, along with the externally applied mmf Θ for $N_s = 10$, $B_{max} = 1.5$ T and $f = 1000$ Hz: (a) $Θ_{Rms}$ due to static hysteresis and (b) $Θ_{Lms}$ due to eddy currents.

vanishes [Fig. 3(b)]. In this case the phase shift between the magnetic flux densities B_{si} also vanishes and is observed only when B_m of the SMSS is not in saturation. Corresponding eddy currents i_{es} in the slices (Fig. 4) display a similar behavior, hence they depend on the change of B in the SMSS.

Fig. 5 shows the calculated mmfs for individual slices regarding $B_{max} = 1.5$ T and $f = 1000$ Hz. The complete mmf Θ in the SMSS is decomposed in the mmf caused by the static hysteresis $Θ_{Rms}$ [Fig. 5(a)] and the mmf caused by eddy currents $Θ_{Lms}$ [Fig. 5(b)] in individual slices. The calculated results show, that the static hysteresis loop dictates the mmf when the SMSS is saturated, whereas in the nonsaturated state both mmfs $\boldsymbol{Θ}_{Rm}$ and $\boldsymbol{Θ}_{Lm}$ contribute more or less equally. The differences between these contributions are in the individual slices, where the mmf $Θ_{Rms}$ is bigger in the outer slices and decreases toward the middle, and the mmf $Θ_{Lms}$ is bigger in the inner slices and decreased toward the edge of the SMSS.

IV. Conclusion

The presented magneto-dynamic model has been validated for a NO SMSS, as very good agreement was obtained between the measured and calculated dynamic hysteresis loops. The model is solving the coupling problem between the magnetic field and the eddy currents inside a thin and long SMSS. The advantages of the discussed model are its simplicity, parametric design, flexibility and computational efficiency. Therefore it could be very suitable for use in engineering. The complexity of the model is easily adapted using an adequate number of slices N_s according to the excitation dynamics. In this way, the best computational performance can be achieved. As the model is relatively easy to understand it also has a great value for teaching purposes. Future work will focus on evaluating the model under arbitrary excitation conditions, arbitrary minor loops, and evaluation for GO SMSS.

Acknowledgment

This paper was supported by ARRS under Projects P2-0115 and L2-4114.

References

[1] S. E. Zirka, Y. I. Moroz, P. Marketos, A. J. Moses, D. C. Jiles, and T. Matsuo, "Generalization of the classical method for calculating dynamic hysteresis loops in grain-oriented electrical steels," *IEEE Trans. Magn.*, vol. 44, no. 9, pp. 2113–2126, Sep. 2008.

[2] S. E. Zirka, Y. I. Moroz, P. Marketos, and A. J. Moses, "Viscosity-based magnetodynamic model of soft magnetic materials," *IEEE Trans. Magn.*, vol. 42, no. 9, pp. 2121–2132, Sep. 2006.

[3] V. Podlogar, B. Klopčič, G. Štumberger, and D. Dolinar, "Magnetic core model of a midfrequency resistance spot welding transformer," *IEEE Trans. Magn.*, vol. 46, no. 2, pp. 602–605, Feb. 2010.

[4] J. Tellinen, "A simple scalar model for magnetic hystersis," *IEEE Trans. Magn.*, vol. 34, no. 4, pp. 2200–2206, Jul. 1998.

[5] D. M. Zhang, Y. T. Liu, and S. Huang, "Differential evolution based parameter identification of static and dynamic J-A models and its application to inrush current study in power converters," *IEEE Trans. Magn.*, vol. 48, no. 11, pp. 3482–3485, Nov. 2012.

[6] F. Henrotte and K. Hameyer, "A dynamical vector hysteresis model based on an energy approach," *IEEE Trans. Magn.*, vol. 42, no. 4, pp. 899–902, Apr. 2006.

[7] S. Bi, A. Sutor, R. Lerch, and Y. Xiao, "An efficient inverted hysteresis model with modified switch operator and differentiable weight function," *IEEE Trans. Magn.*, vol. 49, no. 7, pp. 3175–3178, Jul. 2013.

[8] R. G. Harrison, "Modeling high-order ferromagnetic hysteretic minor loops and spirals using a generalized positive-feedback theory," *IEEE Trans. Magn.*, vol. 48, no. 3, pp. 1115–1129, Mar. 2012.